



CrossMark
click for updates

Cite this: *CrystEngComm*, 2016, 18, 3635

Interplay between poly(ethylene oxide) and poly(L-lactide) blocks during diblock copolymer crystallization

M. L. Arnal,^{*ab} S. Boissé,^b A. J. Müller,^{acd} F. Meyer,^{ef} J.-M. Raquez,^e P. Dubois^e and R. E. Prud'homme^{*b}

The influence of composition and crystallization conditions on the behavior of double crystalline poly(ethylene oxide-*b*-L-lactide) (PEO-*b*-PLLA) diblock copolymers is investigated. Poly(L-lactide) contents in the synthesized copolymers vary from 50 to 91%, and the molecular weight of the PLLA block ranges from 2 to 20 kg mol⁻¹, while that of the PEO block is kept constant at 2 kg mol⁻¹. In bulk samples, DSC results show a synergistic interaction between the crystallization processes of the two blocks. The PEO block provides heterogeneities and exerts a plasticizing action which favors the crystallization of the PLLA block with a nucleation efficiency of 30%. In contrast, the subsequent crystallization of the PEO block is subject to two opposing effects: (a) the nucleating action of PLLA crystals and (b) the topological and geometrical constraints imposed by PLLA crystals, especially when the PEO content is 20 wt% or less. In the case of ultra thin films, block copolymers with PEO contents equal or smaller than 20 wt% form distorted PLLA single crystals when crystallized from the melt. However, upon increasing the PEO content in the system to 33 wt% (by blending or copolymerization), the distortions disappear and the angle between the {110} growth faces changes from 140° to 121°, since the PEO block acts as a solvent or plasticizer for the PLLA block during the crystallization process. PEO incorporation can therefore tailor the rate and morphology of PLLA block crystallization. TEM and AFM studies allowed direct observation of the PEO block dendritic crystals on the surface of lozenge-shaped PLLA crystals previously formed during cooling from the melt.

Received 7th February 2016,
Accepted 22nd April 2016

DOI: 10.1039/c6ce00330c

www.rsc.org/crystengcomm

Introduction

Block copolymers are materials that have applications as thermoplastic elastomers, pressure sensitive adhesives, additives and drug delivery carriers.^{1–3} The ability of block copolymers to self-assemble in the melt according to the relative thermodynamic repulsion between their components has been extensively explored both theoretically and experimentally.^{2,3}

Crystallizable block copolymers in the strong segregation regime exhibit confined crystallization within their micro-

phases that are dictated by composition and thermodynamic repulsion.^{2,4–6} Hence spherulites or any other type of superstructures are not formed. When crystallizable block copolymers are either miscible in the melt or are in the weak segregation regime, crystallization dominates the morphology and upon cooling from the melt, the first block to crystallize can form superstructures (like spherulites or axialites) that template the final morphology. Therefore, factors like chemical structure, molecular weight, molecular architecture, number of crystallizable blocks and crystallization conditions provide a very large number of variables to tailor the morphology and properties of these materials.^{4–7}

In diblock copolymers in which both blocks are crystallizable and miscible in the melt, the block with higher crystallization temperature begins its transformation without confinement while the second block crystallizes under a confined situation within the templated morphology produced by the first block. In this category, poly(ethylene oxide-*b*-L-lactide) (PEO-*b*-PLLA), for example, has been used in suture and scaffolds, as carriers for drug delivery, and for biodegradable stents because it exhibits biodegradability, innocuousness and biocompatibility.^{8–12} Adequate performance in terms of strength and ductility depends on the semi-

^a Grupo de Polímeros USB, Departamento de Ciencia de los Materiales, Universidad Simón Bolívar, Apartado 89000, Caracas 1080-A, Venezuela. E-mail: marnal@usb.ve

^b Département de Chimie, Université de Montréal, Montréal, Québec, H3C 3J7 Canada. E-mail: re.prudhomme@umontreal.ca

^c POLYMAT and Polymer Science and Technology Department, Faculty of Chemistry, University of the Basque Country UPV/EHU, Paseo Manuel de Lardizabal 3, 20018 Donostia-San Sebastián, Spain

^d IKERBASQUE, Basque Foundation for Science, Bilbao, Spain

^e Center of Innovation and Research in Materials & Polymers (CIRMAP), Materials Nova Research Center, Université de Mons, Place du Parc 20, B-7000 Mons, Belgium

^f Laboratory of biopolymers and supramolecular nanomaterials, Faculty of Pharmacy, Université Libre de Bruxelles (ULB), Boulevard du Triomphe, 1050 Bruxelles, Belgium

crystalline structure of the material, as well as the rate of biodegradation. Therefore, the crystallization process and the interplay between the two blocks during the formation of the final structure is of utmost importance. PEO-*b*-PLLA diblock copolymers have been studied previously and the relative miscibility between the two blocks has been reported by several authors who observed only one T_g that changes with composition.^{10,11,13,14} Nevertheless, Rashkov *et al.*¹⁰ pointed out that the observed changes in T_g are small as compared to those expected for full miscibility. In addition, the T_g of the PLLA block is very close to the melting temperature of the PEO block and this situation hampers its observation by thermal techniques.

The crystallization process of the two block components in the bulk has been studied by several authors. Huang *et al.*^{13,14} studied the phase segregation process in PEO-*b*-PLLA block copolymers with PEO weight contents of 24 and 14% by DSC and SAXS and concluded that a disorder-to-order transition occurs driven by the crystallization of the PLLA block. Sun *et al.* and Huang *et al.* reported that the PEO block accelerated the crystallization rate of the PLLA block in block copolymers of various weight compositions, between 7 and 52% of PEO.^{12–15} In contrast, Kim *et al.*¹⁶ showed by time-resolved WAXS that the crystallization of the PLLA block is retarded due to the presence of the PEO block in studying block copolymers with PEO contents between 20 and 66%. For the PEO block crystallization, Yang *et al.*¹⁷ reported an increase in the crystallization rate for the PEO block when its content is between 50 and 67 wt%. Polarized light optical microscopy analysis showed spherulitic superstructures for diblock copolymers of different compositions after PLLA crystallization; the subsequent crystallization of the PEO block did not change significantly the previous superstructure.^{12,13,18,19}

The PEO-*b*-PLLA morphology in thin films has been more rarely evaluated. Yang *et al.*²⁰ studied the morphology of thin films of PEO-*b*-PLLA with a PEO content of 50%, and reported lozenge-spiral dislocations, lozenge multilayers, and hexagonal (or truncated lozenge) multilayer PLLA crystals and PEO dendritic crystals. Huang *et al.*^{13,14} observed lozenge-shaped crystals of PLLA with screw dislocations employing AFM, but the crystalline morphology of the PEO block was not observed using microscopy techniques because of its small size in the block copolymers employed. Similar PLLA crystals were observed after isothermal crystallization by heating from the glassy state (compositions with 24 and 14% of PEO). Sun *et al.*¹² observed by AFM single crystals with an abundance of screw dislocations that were formed during the crystallization of the PLLA blocks. Yang *et al.*^{21,22} proposed that the crystallization kinetics, morphology and crystal orientation of crystalline block copolymer thin films (90 nm) with a PEO content of 50% can be controlled by a prior wetting process.

From the studies cited above for PEO-*b*-PLLA linear diblock copolymers, it is apparent that the crystallization of the two blocks is not completely understood and some con-

tradictory results have been reported. In the present article, using a broader range of compositions than before, we show the complex interplay between the PEO and the PLLA blocks during crystallization of both bulk and thin films. The series used is made of well-defined block copolymers obtained through a metal-free ring-opening polymerization method, in which the PEO block remains constant in molecular weight. In order to vary composition, only the PLLA block length is increased in the copolymers. The role of the PEO block acting as a polymeric diluent or plasticizer will be particularly emphasized.

Experimental

Materials

The typical procedure for the metal-free synthesis of PEO-*b*-PLLA diblock copolymers was previously reported²³ and can be summarized as follows: L-lactide and poly(ethylene glycol) monomethyl ether are dissolved in chloroform, then diazabicyclo undec-7-ene (DBU) is added, and the solution is stirred at room temperature for 10 min. Then, three drops of acetic acid are added, and the resulting mixture is precipitated out in heptane; the poly(ethylene glycol) monomethyl ether was purchased from Fluka, L-lactide was provided by PURAC and its chiral purity was at least 99%. Table 1 lists the molecular weight characterization data obtained by size exclusion chromatography (SEC) and by ¹H NMR. Molecular characterizations of PEO-*b*-PLLA diblock polymers were monitored through the relative number-average molecular weight (M_n) and associated polydispersity indices (PDI) as determined by gel permeation chromatography (GPC) and by ¹H NMR spectroscopy. In all cases, the ¹H NMR spectra revealed a good correlation between theoretical and experimental number-average molecular weights, *i.e.*, PLLA chain lengths of *ca.* 4000, 10 000, and 20 000 g mol⁻¹ from PEO of 2000 g mol⁻¹ and PLLA segments of *ca.* 5000 with a PEO of 5000 g mol⁻¹. Moreover, the narrow PDIs of block copolymers were in the range 1.04–1.11, confirming a good control over the reactions (Table 1). The diblock nomenclature that we have used identifies the PEO block as EO, and the PLLA block as LA; subscripts indicate the composition in wt%, and superscripts the number-average molecular weight of each block in kilograms per mole. For example, EO₃₃²LA₆₇⁴ means: 33% weight percent of PEO and 67% of PLLA; the molecular weight of the former block is 2 kg mol⁻¹ and the molecular weight of the latter is 4 kg mol⁻¹.

Differential scanning calorimetry

A Thermal Analysis Q-2000 DSC was employed. Samples of 3 mg were encapsulated in aluminum pans. The calibration was performed with indium, and ultrapure nitrogen was employed as circulating gas for all tests. Measurements during cooling and heating scans were performed at 10 °C min⁻¹. Degrees of crystallinity, X_c , were calculated from $X_c = \Delta H_m / \Delta H_m^0$ where ΔH_m is the measured enthalpy of fusion (or crystallization) for the block considered, normalized by its

Table 1 Molecular characteristics of block copolymers and homopolymers

Sample	EO/LA ^a (wt%)	M_n EO block (kg mol ⁻¹)	M_n LA block ^b (kg mol ⁻¹)	PDI ^c
EO ₅₀ ² LA ₅₀ ²	50/50	2	2	1.06
EO ₃₃ ² LA ₆₇ ⁴	33/67	2	4	1.06
EO ₂₉ ² LA ₇₁ ⁵	29/71	2	5	1.11
EO ₂₀ ² LA ₈₀ ⁸	20/80	2	8	1.11
EO ₁₇ ² LA ₈₃ ¹⁰	17/83	2	10	1.09
EO ₉ ² LA ₉₁ ²⁰	09/91	2	20	1.11
LA ₄₂ ⁵ EO ₁₆ ² LA ₄₂ ⁵	42/16/42	2	5	1.11
EO ₅₀ ⁵ LA ₅₀ ⁵	50/50	5	5	1.04
PEO ^{2.0}	100/0	2	—	1.05
PEO ^{1.5}	100/0	1.5	—	1.14
PEO ^{4.6}	100/0	4.6	—	—
PLLA ^{4.6}	0/100	—	4.6	1.21

^a Experimental composition as determined by ¹H NMR. ^b Calculated M_n estimated by ¹H NMR for the LA block knowing the M_n of the EO.

^c Polydispersity index of the block copolymer (determined by SEC).

composition and ΔH_m^0 is the enthalpy of fusion of the corresponding 100% crystal structure. ΔH_m^0 values of 206.2 and 92.9 J g⁻¹ were used for PEO and PLA, respectively.^{24,25} In all cases, the measured enthalpy of fusion is given relative to the mass of the block considered (and not the total mass of the sample). The procedure to induce self-nucleation in each block was that described by Fillon *et al.*²⁶ The complete thermal treatment is described as follows: (a) heating and keeping the sample at 170 °C for 3 min to erase previous thermal history; (b) cooling at 10 °C min⁻¹ to -90 °C to create a standard thermal history; (c) partial melting up to a T_s temperature, at which the sample is completely melted, self-nucleated, or self-nucleated and annealed.

If T_s is high enough to fully melt the sample erasing its thermal history, the sample is said to be in “Domain I” or complete melting domain. When T_s is high enough to melt almost completely the sample, but low enough to leave self-nuclei that are able to nucleate the sample during subsequent cooling from T_s , the sample is said to be in “Domain II” or self-nucleation domain. The nature of self-nuclei (whether small crystal fragments remain in the melt or the melt retains segmental orientation caused by crystalline memory effects) depends on the T_s temperature range.^{27,28} When T_s is too low, only part of the crystal population is melted and, therefore, the un-melted crystals are annealed during 3 min at T_s while the rest of the polymer is self-nucleated during the subsequent cooling from T_s ; the sample is then said to be in “Domain III” or self-nucleation and annealing domain; (d) thermal conditioning at T_s during 3 min; (e) DSC cooling scan from T_s , at 10 °C min⁻¹, where the effects of the thermal treatment are reflected on the crystallisation of the PLLA or PEO blocks; (f) DSC heating scan from -90 to 170 °C, at 10 °C min⁻¹, where the effects of the entire thermal history are also reflected in the melting behaviour of each block. Xu *et al.*²⁹ performed self-seeding experiments in poly(2-vinylpyridine-*b*-polyethylene oxide) diblock copolymers (P₂VP-*b*-POE) and poly(ferrocenyl dimethyl silane) (PFS). They claimed that polymer crystallites have a wide range of melting temperatures, enabling para-

doxical phenomena such as the coexistence of melting and crystallization. They reported a self-seeding technique that enables the generation of arrays of orientation-correlated polymer crystals of uniform size and shape (‘clones’) with their orientation inherited from an initial single crystal. Zhang *et al.*³⁰ studied polyethylene single crystals consisting of folded chains that are always in a nonequilibrium state, even if they are faceted. For low-molecular weight polyethylene the formation of the well known “Swiss-cheese” like morphology with randomly distributed holes of varying sizes within the annealed single crystal was observed. Reiter and Sommer^{31,32} reported fingerlike branched crystal patterns with a characteristic width w that resulted from isothermal crystallization at temperatures (T_c) below the melting point (T_m) for polyethylene oxide. They demonstrate that PEO can crystallize, even if it is adsorbed onto a solid surface or confined in thin films. The process is controlled by the crystallization energy and the diffusion process on the surface. It may be called *annealed* diffusion-limited aggregation. Recently Hölzer *et al.*³³ studied crystal thickening during annealing in block copolymers using several techniques: DSC, SAXS and WAXS. They reported three annealing regimes: at low annealing temperature, steady lamellar thickening was found; thermal fractionation was observed at intermediate annealing temperatures due to the exclusion of shorter chains from the crystals; finally, when annealing close to and above the peak melting temperature, self-nucleation of the molten fractions dominated.

Ultrathin film sample preparation

Ultrathin films were prepared by spin coating at a rotation speed of 3000 rpm for 20 s, followed by acceleration to 4000 rpm s⁻¹, using a Headway Research Inc EC-101 apparatus. Dichloromethane was used as solvent. A thickness of 15 nm was obtained from a concentration of 3 mg mL⁻¹. The films were cast onto cleaned Si substrates (p-type single side polished (100) silicon wafers) for the AFM observations. The wafers were cleaned by immersion in dichloromethane for 10

min in an ultrasonic bath to remove any organic contamination. The substrates were dried in nitrogen and, later, by spin-coating for 40 s at 3000 rpm. To keep a solvent-saturated atmosphere around the sample and to allow a uniform evaporation, a glass dome was placed on top of the sample area during spin-coating. Film thicknesses were measured in a Woolam M-2000 ellipsometer. In the case of TEM observations, ultrathin films were spin-coated on freshly cleaved mica substrates covered by a carbon layer (108 carbon/A, Cressington Carbon Coater).

Atomic force microscopy

A Nanoscope III Multimode AFM apparatus (Digital Instrument (DI)), operated in tapping mode and equipped with a high-temperature heating accessory (DI), was used to capture images. J and JVH scanners were used (maximal scan size 20–20 μm) with silicon nitride probes (MikroMasch and Nanosensor).

Two different procedures were employed for AFM observations:

(a) Samples were observed at room temperature after they were subjected to sequential isothermal crystallization for each block in a Linkam hot stage. The diblock copolymer samples were first isothermally crystallized at 120 or 110 $^{\circ}\text{C}$ to promote the PLLA block crystallization, followed by quenching to 30 $^{\circ}\text{C}$, a temperature at which the PEO block crystallization was achieved.

(b) The AFM hot stage accessory was employed to control the temperature while the sample was being observed. The samples were first melted at 170 $^{\circ}\text{C}$ for two minutes and then quenched to 110 or 100 $^{\circ}\text{C}$ to crystallize the PLLA block under isothermal conditions for 3 h. Then, samples were quenched to 30 $^{\circ}\text{C}$ and left at that temperature to promote the crystallization of the PEO block. Holding times of 3 to 18 h at 30 $^{\circ}\text{C}$ were implemented. Once the crystallization step at 30 $^{\circ}\text{C}$ was completed, the samples were reheated in the AFM hot stage to 70 $^{\circ}\text{C}$, in order to melt the PEO blocks. Micrographs and analysis at this temperature were performed. The comparison of the images obtained at different temperatures, as well as image analysis (designed to determine sample heights as a function of the crystallization temperature) were employed to distinguish the crystalline morphology corresponding to each block. During all thermal treatments, the AFM probe was maintained at the same temperature as the sample to avoid any condensation.

AFM scan rates of 1 and 0.5 Hz were employed.

Transmission electron microscopy

A Phillips Tecnai H transmission electron microscope (TEM) operating at 80–100 kV was used for the TEM and electron diffraction experiments. Films were melted for 2 min at 170 $^{\circ}\text{C}$ and crystallized on mica in a two-step procedure in a THMS-600 Linkam hot stage connected to a TMS94 temperature controller. After crystallization, samples (on mica) were placed on an ice bath. The films were separated from the

mica by floating them in water, and they were transferred to copper grids for observation.

Results and discussion

Non-isothermal crystallization of bulk block copolymer samples

PEO-*b*-PLLA block copolymers of relatively low molecular weight have been reported as miscible or partially miscible.⁶ The PEO melting temperature and PLLA glass transition temperature are very close, and their signals superpose and cannot be used to verify the miscibility. However, the product of the Flory–Huggins interaction parameter (χ), estimated from the solubility parameters of the two blocks ($\delta_{\text{PEO}} = 21 \text{ J cm}^{-3}$ and $\delta_{\text{PLA}} = 20.2 \text{ J cm}^{-3}$),^{34,35} by the degree of polymerization of the copolymer N can be used as a first approximation to estimate the degree of segregation between the blocks. For the system EO-*b*-LA, values of 1.6 and 7.4 were obtained for the product χN at 100 $^{\circ}\text{C}$ considering a total degree of polymerization of 4 and 22 kg mol^{-1} , respectively. These values are below $\chi N = 10$ which is considered the boundary between weak and intermediate segregation regimes.³⁶

DSC results

Fig. 1.a shows the DSC cooling scans of PEO-*b*-PLLA diblock copolymers in which the PEO block length remains constant at 2 kg mol^{-1} while the PLLA block length increases from 2 to 20 kg mol^{-1} . For comparison purposes, the DSC scans of representative homopolymers are also reported. For the majority of the block copolymers, two exotherms are observed. The first signal, at higher temperatures, corresponds to the PLLA block crystallization from the melt, and the second one, at lower temperatures, corresponds to the crystallization of the PEO block. This second step takes place in a two-phase system made of a PLLA crystal phase and a miscible or partially miscible amorphous phase (composed of PLLA and PEO

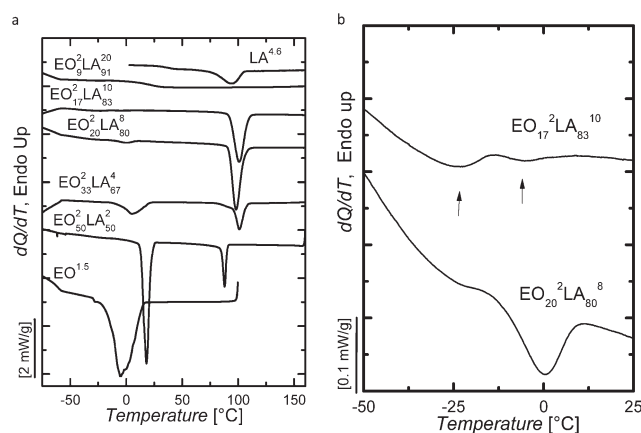


Fig. 1 a DSC cooling scans at 10 $^{\circ}\text{C min}^{-1}$ for homopolymers and block copolymers $\text{EO}_x^y\text{LA}_x^y$ after melting for 3 min at 170 $^{\circ}\text{C}$. b Fractionated crystallization in DSC cooling scans at 10 $^{\circ}\text{C min}^{-1}$ for block copolymers $\text{EO}_{20}^2\text{LA}_{80}^8$ and $\text{EO}_{17}^2\text{LA}_{83}^{10}$ after melting for 3 min at 170 $^{\circ}\text{C}$.

chains). In miscible or weakly segregated bulk block copolymers, like PCL-*b*-PLLA or the present system, PEO-*b*-PLLA, previous studies^{6,21,37,38} by Zhou *et al.*³⁸ have demonstrated that upon cooling from the melt, the PLLA forms spherulites that template the block copolymer morphology, since the second block that crystallizes at much lower temperatures (*i.e.*, PCL or PEO) is forced to crystallize in the interlamellar and/or interfibrillar regions. When the PLLA block content is large, the second block may experience confinement leading to fractionated crystallization (see below). In addition, crystallization of most polymers is accompanied by the separation of different molecular species, a process referred to as molecular fractionation. In linear polyethylene, fractionation occurs due to differences in molar mass. The low molar mass material crystallizes at low temperatures in subsidiary lamellae. Polymers with branching or tacticity exhibit not only molar mass segregation but also segregation phenomena relating to structural irregularities.³⁹

Fig. 1.a and Table 2 illustrate that the PLLA homopolymer with an $M_n = 4.6 \text{ kg mol}^{-1}$ partially crystallizes during cooling with a peak crystallization temperature, T_c , of 93.9 °C whereas, in the diblock copolymer $\text{EO}_{33}^2\text{LA}_{67}^4$, for a similar PLLA block molecular weight, the T_c is 100.6 °C, a value 7 °C higher than that of the homopolymer. Similar results are observed for the other copolymers of the same series with higher PLLA contents (Table 2).

This trend is explained by the presence of the miscible PEO block that promotes crystallization by a combination of plasticizing action and heterogeneities donation that leads to an efficient nucleating action on PLLA blocks (a more detailed study of this point will be shown in section 3.2 where self-nucleation experiments are presented). For the block copolymer $\text{EO}_9^2\text{LA}_{91}^{20}$, the PLLA block does not crystallize when cooling from the melt as a consequence of the high molecular weight and relative stiffness of the PLLA block. Only the T_g of the block copolymer is observed at 26.1 °C.

Moreover, Fig. 1.a shows that PEO block crystallization in the copolymer is also affected by the PLLA block length. The crystallization temperature of the PEO block is equal or higher than the crystallization temperature of the PEO homopolymer of molecular weight 1.5 kg mol^{-1} . This is a consequence of the higher molecular weight of the PEO block in the copolymers and also a consequence of the nucleating action of PLLA crystals on the PEO chains. However, since the

system is weakly segregated or partially miscible, the stiffness of the amorphous phase increases with PLLA content hindering PEO block crystallization. For PEO contents between 15% to 20%, two crystallization exotherms at higher supercoolings are observed (−25.6 °C and −5.9 °C, see Fig. 1.b for $\text{EO}_{17}^2\text{LA}_{83}^{10}$) while, for $\text{EO}_{20}^2\text{LA}_{80}^8$, a small signal close to −25 °C is observed in addition to a large peak at 0.6 °C. PEO block confinement can explain this characteristic behaviour that is called fractionated crystallization. For PEO contents below 10% crystallization is not observed. The term fractionated crystallization means that the crystallization process takes place in a series of isolated microdomains at different temperatures in an independent way. It happens as a consequence of the confinement of a semi-crystalline polymer that is dispersed in a non-nucleating matrix, in which the number of microdomains is higher than the number of active heterogeneous nuclei in the bulk polymer. Different domains can contain different types of heterogeneities with variable efficiency to promote crystallization at different supercoolings. This phenomenon has been reported for immiscible and miscible blends, and for melt segregated and melt miscible block copolymers.^{40–44} During crystallization, fractionation as a consequence of the molecular weight distribution of the homopolymer or block that crystallizes takes place.^{40–44} Nevertheless this type of fractionation happens for all 2K EO blocks in the copolymers because the molecular weight distribution of these PEO blocks is exactly the same for all samples. DSC cooling scans show that fractionated crystallization only takes place for PEO block in block copolymers ($\text{EO}_{17}^2\text{LA}_{83}^{10}$, $\text{EO}_{20}^2\text{LA}_{80}^8$) where isolated domains are generated as a consequence of composition.

In the present case, when the PEO content is low, the PEO chain segments are isolated from the PLLA crystals (that were formed previously templating the morphology) and from heterogeneities active at low supercoolings and, therefore, crystallization takes place at higher supercoolings. The PEO block in the copolymer $\text{EO}_9^2\text{LA}_{91}^{20}$ does not crystallize because the system exhibits a high T_g of 26.1 °C, a value that is close to the melting of PEO crystals, therefore reducing the probability to form stable nuclei under non-isothermal conditions (*i.e.*, cooling at 10 °C min^{-1}). Tables 2–4 summarize the crystallization and melting temperatures, and degrees of crystallinity of homopolymers and copolymers evaluated.

PEO-*b*-PLLA block copolymers are reported as partially miscible or weakly segregated systems. A higher miscibility is expected for low molecular weight block copolymers, in this case only one T_g may be expected. The measurement of T_g by DSC is quite complex for these block copolymers because the melting signal of PEO block is close to the T_g signal for the PLLA block. The complex trend for the T_g reported in Table 2 suggests that miscibility between blocks decreases with increases in molecular weight. The reported T_g value corresponds to the poly(ethylene oxide) rich amorphous phase for $\text{EO}_{29}^2\text{LA}_{71}^5$, $\text{EO}_{20}^2\text{LA}_{80}^8$ and $\text{EO}_{17}^2\text{LA}_{83}^{10}$ block copolymers (on the opposite composition side, for $\text{EO}_9^2\text{LA}_{91}^{20}$, the reported T_g corresponds with the PLLA amorphous rich phase).

Table 2 Thermal transitions of the LA block of PEO-*b*-PLLA block copolymers

Sample	T_g (°C)	T_c (°C)	T_m (°C)
PLLA ^{4,6}	41.7	93.9	129.4
$\text{EO}_{50}^2\text{LA}_{50}^2$	−29.1	87.6	110.6
$\text{EO}_{33}^2\text{LA}_{67}^4$	−29.5	100.6	134.9
$\text{EO}_{29}^2\text{LA}_{71}^5$	−35.7	85.9	136.2
$\text{EO}_{20}^2\text{LA}_{80}^8$	−41.8	97.6	145.1
$\text{EO}_{17}^2\text{LA}_{83}^{10}$	−41.6	99.8	141.2
$\text{EO}_9^2\text{LA}_{91}^{20}$	26.1	—	138.3
$\text{EO}_{50}^5\text{LA}_{50}^5$	n.d.	85.7	130.5
$\text{LA}_{42}^5\text{EO}_{16}^2\text{LA}_{42}^5$	−29.3	101.9	141.1

Fig. 2 shows the heating scans of all copolymers and homopolymers. Two samples exhibit cold crystallization: the LA^{4.6} homopolymer and EO₉²LA₉₁²⁰ copolymer. In contrast, the copolymers where the PLLA block molecular weights range from 2 to 10 kg mol⁻¹ do not exhibit cold crystallization; the combination of nucleating activity of new heterogeneities (*i.e.*, impurities transferred from the PEO blocks) and the PEO block plasticizing action, allows the crystallization to take place during the previous cooling, unlike the homopolymer whose crystallization rate is lower.

The melting temperatures of all PEO blocks are higher than that observed for the 1.6 kg mol⁻¹ PEO homopolymer (Table 3), with a slight tendency to decrease as the PEO content in the block copolymer decreases and while, in addition, the degree of confinement promoted by PLLA crystals and the more rigid amorphous phase increase.

In the case of the melting behaviour of the PLLA blocks (Table 2), their melting temperatures are also higher than that observed for PLLA. This trend is clearly seen when comparing samples with similar molecular weights, for example PLLA^{4.6} with $T_m = 129.4$ °C, and EO₃₃²LA₆₇⁴ or EO₂₉²LA₇₁⁵ with $T_m = 134.9$ and 136.2 °C, respectively.

However, for EO₁₇²LA₈₃¹⁰ and EO₉²LA₉₁²⁰ samples, the trend is reversed and there is a decrease of T_m (relative to EO₂₀²LA₈₀⁸) as expected from the confinement degree experienced by the PEO blocks, which have to crystallize in a fractionated fashion (EO₁₇²LA₈₃¹⁰) or from the glassy state *via* cold crystallization (EO₉²LA₉₁²⁰). For EO₉²LA₉₁²⁰ the thermal history is different from the other samples because all the crystallization process takes place during the heating scan (cold crystallization). As a consequence of the relative stiffness of the PLLA block and kinetic reasons, it is not possible for this block to crystallize from the melt during the cooling step. For all the other samples, crystallization from the melt is allowed as a consequence of the combination of a higher proportion of PEO block and a lower molecular weight for the PLLA block.

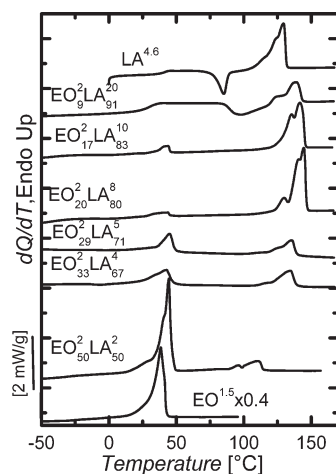


Fig. 2 DSC heating scans at 10 °C min⁻¹ for homopolymers and block copolymers EO_x^yLA_x^y after cooling scans presented in Fig. 1.

Table 3 Thermal transitions of the EO block of PEO-*b*-PLLA block copolymers

Sample	T_g (°C)	T_c (°C)	T_m (°C)
PEO ^{1.5}	-63.4	-5.2	38.5
PEO ^{4.6}	-53.0	40.7	58.5
EO ₅₀ ² LA ₅₀ ²	-29.1	17.9	44.6
EO ₃₃ ² LA ₆₇ ⁴	-29.5	4.6	43.0
EO ₂₉ ² LA ₇₁ ⁵	-35.7	10.5	45.6
EO ₂₀ ² LA ₈₀ ⁸	-41.8	-25.0; 0.6	44.3
EO ₁₇ ² LA ₈₃ ¹⁰	-41.6	-25.6; -5.9	44.8
EO ₉ ² LA ₉₁ ²⁰	26.1	—	—
EO ₅₀ ³ LA ₅₀ ⁵	n.d.	28.2	53.0
LA ₄₂ ⁵ EO ₁₆ ² LA ₄₂ ⁵	-29.3	—	—

Concerning the degrees of crystallinity calculated from the DSC enthalpies of fusion, for the PLLA block (Table 4), the general trend is that the larger the PLLA content, the larger X_c (with the exception of EO₉²LA₉₁²⁰). X_c values calculated from the melting peak are the sum of crystallization during previous cooling run plus the crystallization during heating (*i.e.*, cold crystallization). Table 4 indicates that, often, for the copolymers, most of the crystallization occurs in the cooling step (except for EO₉²LA₉₁²⁰). For the PEO block (Table 4), X_c decreases with the PEO content, despite the fact that all samples have the same PEO block molecular weight, because the PLLA block crystallizes first, followed by the crystallization of the PEO block at lower temperatures: the higher the PLLA content, the more difficult the crystallization of the PEO block, that must occur within the template established by PLLA spherulites.

Self-nucleation experiments on bulk block copolymer samples

The above DSC results show that the presence of the PEO block in the block copolymer enhances PLLA block crystallization. In order to study more deeply this phenomenon, self-nucleation experiments were performed on homopolymer

Table 4 Degree of crystallinity determined by DSC

Sample	PLLA block		PEO block	
	X_c^a (%)	X_c^b (%)	X_c^a (%)	X_c^b (%)
PLLA ^{4.6}	30	54	—	—
PEO ^{1.5}	—	—	75	69
PEO ^{4.6}	—	—	90	79
EO ₅₀ ² LA ₅₀ ²	20	20	47	55
EO ₃₃ ² LA ₆₇ ⁴	20	27	27	28
EO ₂₉ ² LA ₇₁ ⁵	21	22	22	25
EO ₂₀ ² LA ₈₀ ⁸	50	57	4.4	11
EO ₁₇ ² LA ₈₃ ¹⁰	53	59	0.2	7.1
EO ₉ ² LA ₉₁ ²⁰	—	24	—	—
EO ₅₀ ³ LA ₅₀ ⁵	35	26	70	73
LA ₄₂ ⁵ EO ₁₆ ² LA ₄₂ ⁵	49	54	—	—

^a Degree of crystallinity calculated considering the crystallization enthalpy. ^b Degree of crystallinity calculated considering the melting enthalpy.

LA^{4.6} and block copolymer EO₃₃²LA₆₇⁴ of similar PLLA block lengths, as shown in Fig. 3 and 4.

Fig. 3 shows the DSC cooling scans after the self-nucleation of LA^{4.6} at 170 °C, and at several T_s temperatures between 146 to 130 °C for 3 min. When the self-nucleation temperature (T_s) is 170 or 146 °C, the crystallization temperature remains the same.

This behaviour indicates that the concentration of heterogeneous nuclei remains constant in that temperature range and this defines Domain I or the heterogeneous nucleation domain according to Fillon *et al.*^{26,45}

An increase in the crystallization temperature is observed after self-nucleation in the 142–130 °C range as shown in Fig. 3 (cooling traces at T_s values of 134, 132, 131, 130 °C). Fig. 4 shows the subsequent melting traces after the cooling scans presented in Fig. 3. Analyzing the results of Fig. 3 and 4, the assignment of the DSC traces to DII or DIII was made, as samples in Domain III exhibit melting of annealed crystals. In Domain II, the exponential increase in nucleation density produced by self-seeding induces higher crystallization temperature (Fig. 3). The temperature interval of T_s values between 142 and 132 °C belongs to Domain II or self-nucleation domain²⁶ However, at T_s values of 130 and 131 °C, an additional change is observed: in the heating curves (Fig. 4), a new melting signal appears at higher temperatures. This new melting endotherm is related to the melting process of the crystals whose thickness increases during the isothermal treatment of 3 min at T_s . The size of this new signal increases as the amount of annealed crystals increases. It is small at $T_s = 131$ °C but larger at 130 °C. Above $T_s = 131$ °C, only slight changes in the shape of the traces are observed.

The same type of experiments was performed for EO₃₃²LA₆₇⁴, with similar results, except that the small annealing peak at high temperatures was found for a T_s of 136 and 137 °C instead of 130 and 131 °C. The shift of the transition from Domain II to Domain III to higher temperatures in the EO₃₃²LA₆₇⁴ copolymer relative to the LA^{4.6} homo-

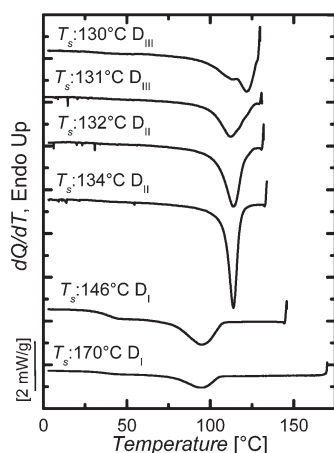


Fig. 3 Self-nucleation experiments for LA^{4.6}: cooling scans at 10 °C min⁻¹. DI, DII and DIII mean Domain I, Domain II and Domain III, respectively.

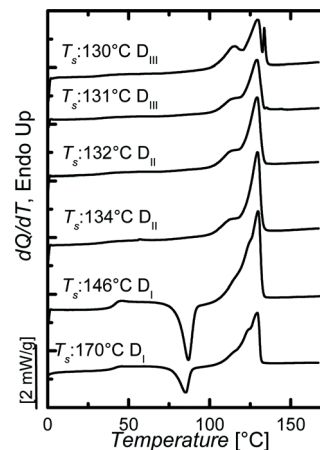


Fig. 4 Self-nucleation experiments for LA^{4.6} heating scans at 10 °C min⁻¹. DI, DII and DIII mean Domain I, Domain II and Domain III, respectively.

polymer is due to the higher melting point of the PLLA block crystals in the copolymer, which therefore have the ability to anneal at higher temperatures.

Self-nucleation experiments can be used to evaluate the efficiency of a nucleating agent in a polymer. Fillon *et al.*⁴⁵ designed a scale for measuring the nucleation efficiency (NE) of heterogeneities through eqn (1):

$$NE = \frac{T_{cNA} - T_c}{T_{cSN} - T_c} \times 100 \quad (1)$$

where T_{cNA} is the crystallization temperature in presence of the nucleating agent, T_c the crystallization temperature without nucleating agent or self-nucleation, and T_{cSN} the crystallization temperature after ideal self-nucleation or self-nucleation obtained with the lowest T_s temperature of Domain II.

Eqn (1) has been used in the literature to quantitatively compare the changes in crystallization temperatures when nucleating agents are added to a homopolymer. In this work, a comparison between the PLLA homopolymer and the PLLA block in the copolymer was done, where the heterogeneities donated by the PEO block act as the nucleating agent. To calculate NE, the following values were considered: T_{cNA} was taken as 100.3 °C (Table 2) for the EO₃₃²LL₆₇⁴ block copolymer and $T_c = 93.9$ °C (Table 2) for the homopolymer. After self-nucleation at 132 °C, the T_{cSN} observed for the homopolymer is 113.1 °C (Fig. 1.a and 3) leading to a nucleation efficiency of 33% by the incorporation of the PEO block in the copolymer. This efficiency is comparable with a value of 32% obtained when 1% of talc is added to PP.⁴⁵ The nucleation efficiency was calculated assuming the simplest situation: that the covalent linkage between both blocks does not affect the crystallization. Nevertheless, nucleation and antinucleation effects have been reported. In addition coincident, sequential and fractionated crystallization have been observed in block copolymer with two or more crystallizable blocks.^{4,6,42–44,46,47}

Xu *et al.*,²⁹ Zhang *et al.*,³⁰ Reiter and Sommer^{31,32} also report interesting results using self-nucleation and self-seeding techniques.

Thin films morphology by AFM

The solid-state morphology of the copolymers was studied in films having thicknesses between 10 and 15 nm as determined by ellipsometry. Isothermal treatments were conducted at 100 and 110 °C for several hours to promote the crystallization of the poly(L-lactide) block, followed by storage at room temperature where the PEO block can crystallize. Reiter and Sommer reported fingerlike branched crystal patterns with a characteristic width w that resulted from isothermal crystallization at temperatures (T_c) below the melting point (T_m) for polyethylene oxide. They demonstrate that PEO can crystallize, even if it is adsorbed onto a solid surface or confined in thin films. The process is controlled by the crystallization energy and the diffusion process on the surface. It may be called *annealed* diffusion-limited aggregation.^{31,32}

Fig. 5 shows the crystal morphology obtained after an isothermal crystallization from the melt for 3 h at 110 °C and after the samples were stored at room temperature. All copolymers exhibit single crystal type morphologies.

Surprisingly, crystals with sharper edges are obtained for the copolymers containing less than 80% PLLA, whereas those with 80% or more PLLA show ill-defined boundaries. As shown in Fig. 5, $\text{EO}_{33}^2\text{LA}_{67}^4$ shows a lozenge shape (with multilayers) whereas $\text{EO}_{29}^2\text{LA}_{71}^5$ exhibits simultaneously lozenge and truncated lozenge shapes. Crystals with well-defined {110} and {100} facets are usually obtained at low crystallization temperatures from solution.^{48,49}

In contrast, $\text{EO}_{20}^2\text{LA}_{80}^8$, $\text{EO}_{17}^2\text{LA}_{83}^{10}$ and $\text{EO}_9^2\text{LA}_{91}^{20}$ copolymers exhibit distorted lozenge shape crystals (Fig. 5c–e); in addition, $\text{EO}_9^2\text{LA}_{91}^{20}$ shows a twin crystal morphology (Fig. 5e). As discussed earlier, the PEO block acts as a solvent or plasticizer for the PLLA block during the crystallization process. Therefore, after crystallization from the melt, lozenge-shaped single crystals of PLLA are obtained in samples containing a fair amount of PEO (the angles between facets will be discussed below). It should be noted that the $\text{EO}_{50}^2\text{LA}_{50}^2$ copolymer does not crystallize at 110 °C.

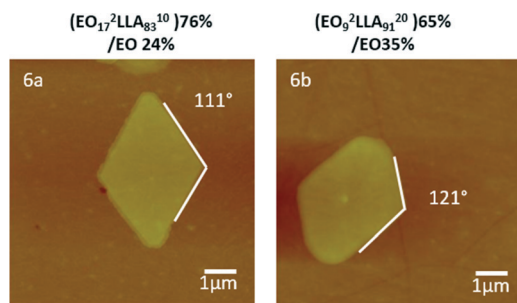


Fig. 6 AFM height images of lamellar crystals obtained for blends between block copolymers and PEO homopolymer after isothermal crystallization at 110 °C. The whole PEO content in both blends is 33%.

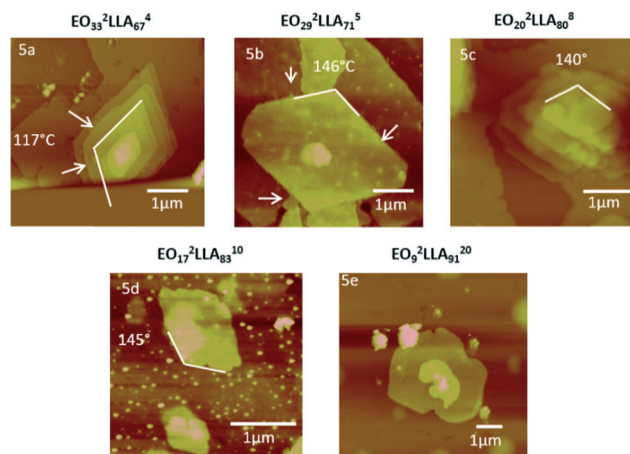


Fig. 5 AFM height images of lamellar crystals obtained for the indicated block copolymers after isothermal crystallization at 110 °C for 3 hours followed by storage at room temperature.

Single crystals are usually obtained from solution crystallization; more recently, in thin films and using high crystallization temperatures, lozenge crystals have been observed in several homopolymers and block copolymers. In this case, segments of chains with shorter stereo-sequences and/or low molecular weight chains act as a solvent for the longest stereo-sequences. In PEO-*b*-PLLA block copolymers, several authors have reported single crystal morphology from the melt.^{12–14,20,22}

In this work, single crystal morphologies for PLLA blocks are observed at several copolymer compositions; and the presence of the PEO block acting as a plasticizer enhances this possibility. Therefore, more regular crystals are obtained for block copolymers with a high PEO content. In addition, if the molecular weight of the PLLA block is not too high, the entanglement density should be low and the PLLA block chains should diffuse more easily to the growth front. On the contrary, when the molecular weight of the PLLA block increases and the entanglement density is larger, the single crystals obtained are less regular, more distorted, and their size and their number are smaller.

A detailed examination of Fig. 5a and b shows the presence of a new layer on the edge of the crystals for $\text{EO}_{33}^2\text{LA}_{67}^4$ and $\text{EO}_{29}^2\text{LA}_{71}^5$ block copolymers (see arrows in the AFM micrographs), which is not seen for the more asymmetric block copolymers containing less PEO (Fig. 5d and e). This observation suggests that the PEO block crystallization mainly takes place in the more symmetric block copolymers thin films in accordance to the DSC results of the bulk polymers (Table 4) that show a very low degree of crystallinity for $\text{EO}_{20}\text{LA}_{80}$ and $\text{EO}_{17}\text{LA}_{83}$. For highly asymmetric copolymers, the PEO block crystallization is double hindered as a consequence of mobility restrictions of the PEO block chains that are covalently linked to previously crystallized PLLA chains (into lozenge shaped crystals) and additional restrictions imposed by the film thickness. In the bulk, without thickness restrictions, the PEO block can crystallize in a wider range of

Table 5 Measured and calculated thicknesses for several layers in PEO-*b*-PLLA block copolymers after isothermal crystallization at 110 °C

Sample	Maximum length of each block (nm)	Sample thickness (nm)	Overall crystal thickness measured (nm)	LA crystal layer thickness calculated (nm)	EO rich highly amorphous layer thickness calculated (nm)
EO ₃₃ ² LA ₆₇ ⁴	13- <i>b</i> -16	13	12 ± 3	7.6	2.2
EO ₂₉ ² LA ₇₁ ⁵	13- <i>b</i> -20	9	12 ± 3	8.2	1.9
EO ₂₀ ² LA ₈₀ ⁸	13- <i>b</i> -32	13	10 ± 2	7.8	1.1
EO ₁₇ ² LA ₈₃ ¹⁰	13- <i>b</i> -40	16	10 ± 2	8.0	1.0
EO ₉ ² LA ₉₁ ²⁰	13- <i>b</i> -80	15	10 ± 2	9.0	0.5
LA ₄₂ ⁵ EO ₁₆ ² LA ₄₂ ⁵	20- <i>b</i> -13- <i>b</i> -20	13	12 ± 4	9.8	1.1
LA ^{4,6}	20	16	10 ± 1	—	—

compositions that includes the EO₁₇²LA₈₃¹⁰ block copolymer (Table 3).

As mentioned above, single crystals of EO₁₇²LA₈₃¹⁰ (Fig. 5d) and EO₉²LA₉₁²⁰ (Fig. 5e) copolymers exhibit an irregular appearance. In order to promote the formation of more

regular crystals with sharp edges, films were prepared from mixtures of each copolymer with PEO homopolymer in order to adjust the overall composition of the systems to 33% PEO content and 67% PLLA content. Fig. 6a and b show AFM images of the crystals formed using blends of EO₁₇²LA₈₃¹⁰ and

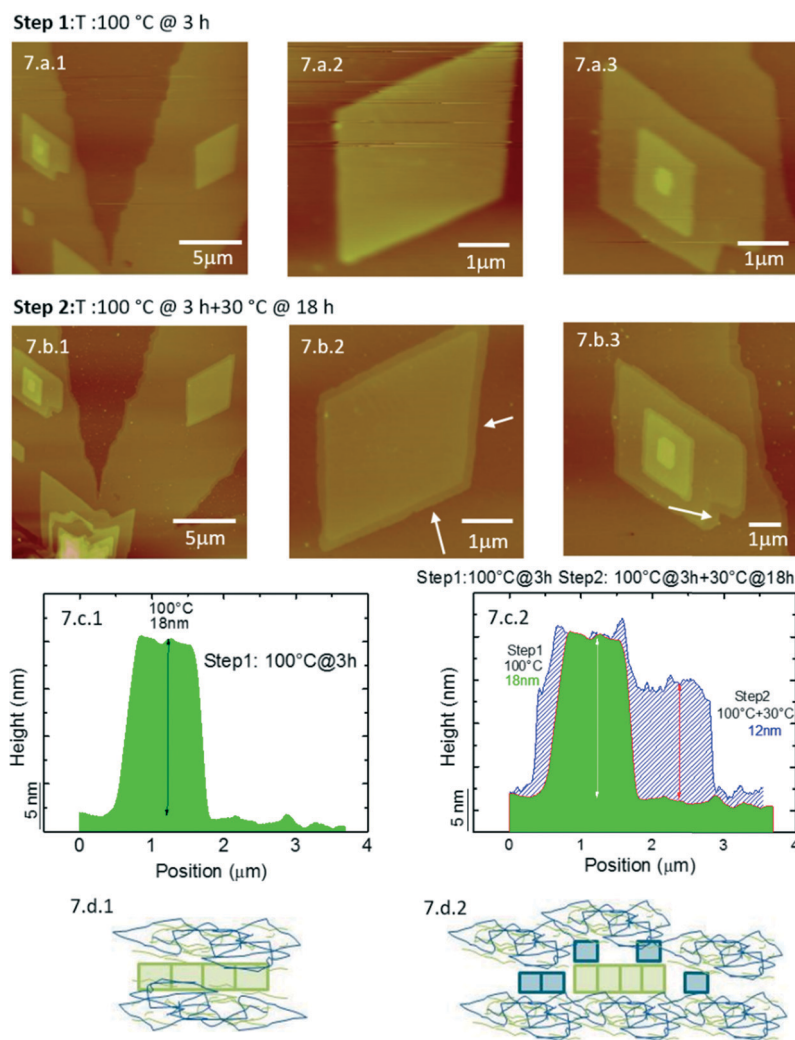


Fig. 7 Evolution of semi-crystalline structure with temperature for EO₅₀⁵LA₅₀⁵ diblock copolymers. Frames 7.a.1, 7.a.2 and 7.a.3 show images obtained after 3 h at 100 °C; frames 7.b.1, 7.b.2 and 7.b.3 show images obtained after 3 h at 100 °C + 18 h at 30 °C. Frames 7.c.1 and 7.c.2 show AFM height traces: the first one in green color is the trace after crystallization at 100 °C. The second one in blue shaded color is the trace after the two steps of crystallization 100 °C + 18 h at 30 °C. Frames 7.d.1 and 7.d.2 are schematic cartoons (green color PLLA block chains and crystals; blue color PEO block chains and crystals).

$\text{EO}_9^2\text{LA}_{91}^{20}$ block copolymers with PEO homopolymer, respectively. They are lozenge-shaped and truncated lozenge-shaped single crystals, very similar to those observed in Fig. 5a and b for $\text{EO}_{33}^2\text{LA}_{67}^4$ and $\text{EO}_{29}^2\text{LA}_{71}^5$, respectively. The disappearance of the distortions in the crystals by PEO addition is indicative of the effectiveness of the PEO component within the copolymers, to obtain crystals similar to those observed in crystallization from solution. This emphasizes the fact that PEO acts as a plasticizer that favours the regular crystallization of the PLLA block

The angle reported in PLLA lozenge-like crystals between the $\{110\}$ faces,⁴⁹ when crystallized in the α form, is 120° , a value similar to that observed (*i.e.*, 117°) for $\text{EO}_{33}^2\text{LA}_{67}^4$ crystals (Fig. 5a). However, for the block copolymers with higher PLLA contents, the angles between the facets are close to 140° (Fig. 5b–d). After the addition of PEO homopolymer, the

angle between the faces becomes 111° in $\text{EO}_{17}^2\text{LA}_{83}^{10}$ and 121° in $\text{EO}_9^2\text{LA}_{91}^{20}$ (Fig. 6a and b). Moreover, in the distorted crystal, the edges tend to be irregular but, after the incorporation of a higher content of PEO by blending, these edges become straighter.

From Fig. 5a–e, the thickness of the single crystals covered by the PEO block can be measured by AFM (at room temperature). Table 5 shows these values, along with the length of each crystallizable block, which depends on the molecular weight and type of crystalline structure, and the thickness of the films measured by ellipsometry. The PLLA single crystals are likely covered or sandwiched by two layers that are richer in the PEO block covalently bound to the PLLA chains. Depending on the block length and storage conditions, these layers may be completely amorphous (PEO and PLLA chains) or partially crystalline PEO structure mixed with amorphous PEO and PLLA

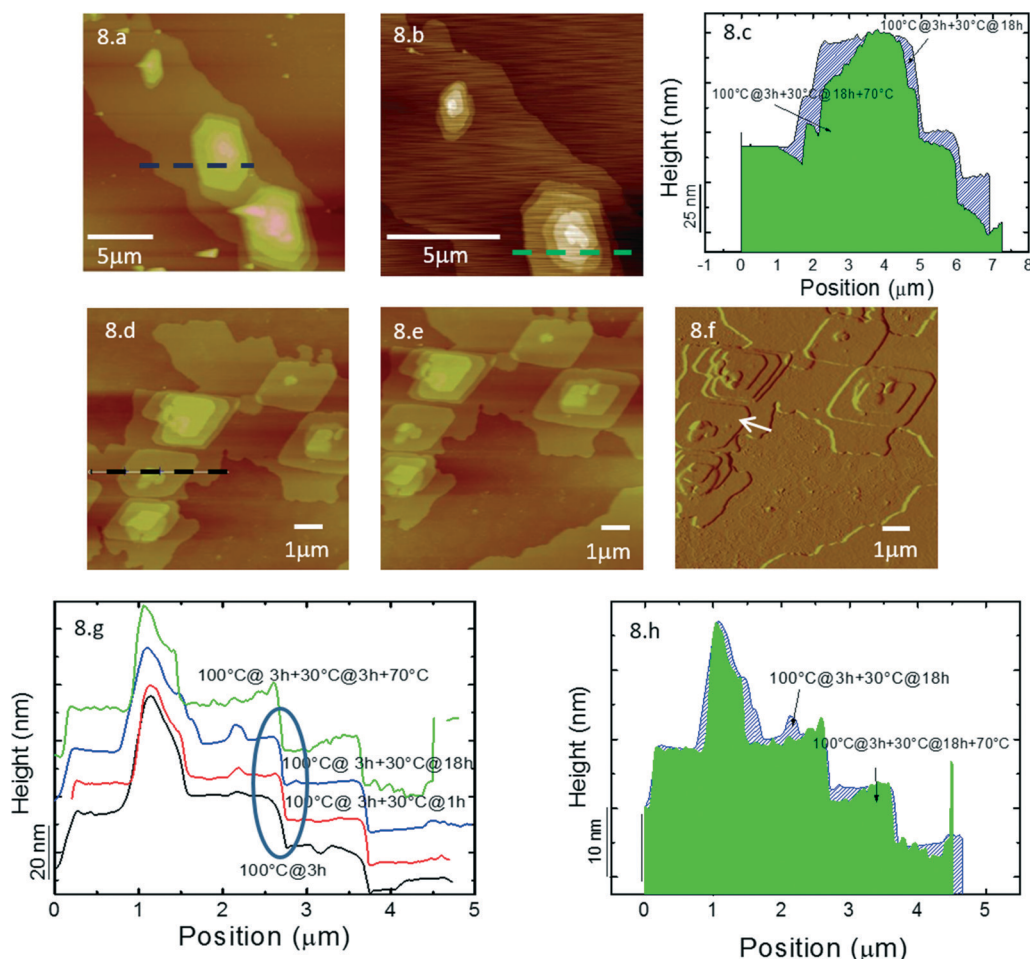


Fig. 8 Evolution of semi-crystalline structure with temperature for $\text{EO}_{33}^2\text{LA}_{67}^4$ diblock copolymers. Frame 8.a shows images obtained after 3 h at 100°C + 18 h at 30°C ; frame 8.b shows images obtained after 3 h at 100°C + 18 h at 30°C + 3 min at 70°C . Frame 8.c shows AFM height traces: the first one in blue shaded color is the trace after the two steps of crystallization 100°C + 18 h at 30°C ; the second one in green color is the trace after the following thermal treatment 100°C + 18 h at 30°C + 3 min at 70°C min, the last step induces the melting of PEO crystals. Frame 8.d shows image obtained after 3 h at 100°C ; frame 8.e and 8.f show images obtained after 3 h at 100°C + 3 h at 30°C (height and amplitude respectively); frame 8.g shows four AFM height traces: the first one after treatment at 100°C , second one at the beginning of 30°C treatment, third one after 2 h 45 min at 30°C , and the fourth one at 70°C in order to melt the EO crystals. Frame 8.h shows two AFM height traces: the first one in blue shaded color is the trace after the two steps of crystallization 100°C + 18 h at 30°C ; the second one in green color is the trace after the following thermal treatment 100°C + 18 h at 30°C + 3 min at 70°C min.

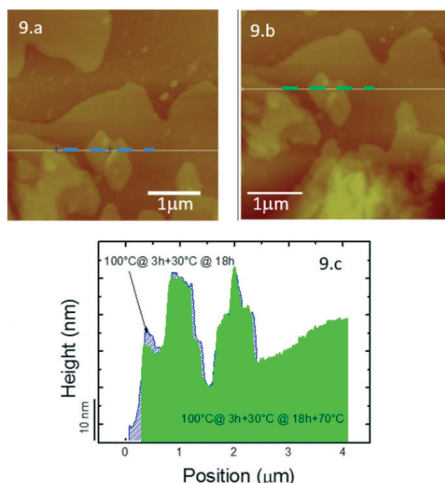


Fig. 9 Evolution of semi-crystalline structure with temperature for $\text{EO}_{20}^2\text{LA}_{80}^8$ diblock copolymers. Frame 9.a. shows the height images obtained after 3 h at 100 °C + 15 h at 30 °C; frame 9.b. shows the height images obtained after 3 h at 100 °C + 15 h at 30 °C + 70 °C; frame 9.c shows two AFM traces: the first one in blue shaded color is the trace after crystallization at 100 °C and 30 °C; the second one, in green, was obtained after heating the sample at 70 °C in order to melt the PEO crystals.

chains. The total measured thickness of the PLLA structure single crystal is between 10 and 12 nm in all cases.

Applying the equation proposed by Chen *et al.*⁵⁰ (eqn 2), the reported thickness determined by AFM in Table 5 can be decomposed into three components: the PEO block rich layer which is in contact with the substrate, the single crystal formed by the PLLA chains (d_{PLLA}^*), and a second PEO block rich layer on top of the crystal. To calculate the thickness of the PLLA single crystal (d_{PLLA}^*), using the total thickness of the covered structure (d_{overall}), eqn (2) was used:

$$d_{\text{PLLA}}^* = \frac{\frac{d_{\text{overall}} M_n^{\text{PLLA}}}{(W_{\text{PLLA}}^c \rho_{\text{PLLA}}^c + W_{\text{PLLA}}^a \rho_{\text{PLLA}}^a)}}{\frac{M_n^{\text{PLLA}}}{(W_{\text{PLLA}}^c \rho_{\text{PLLA}}^c + W_{\text{PLLA}}^a \rho_{\text{PLLA}}^a)} + \frac{M_n^{\text{PEO}}}{\rho_{\text{PEO}}}} \quad (2)$$

where M_n^{PLLA} is the PLLA block number-average molecular weight, W_{PLLA}^c the PLLA crystalline weight fraction, ρ_{PLLA}^c the PLLA crystalline density (1.290 g cm^{-3}),²³ W_{PLLA}^a the PLLA amorphous weight fraction, ρ_{PLLA}^a the PLLA amorphous density (1.248 g cm^{-3}),²¹ M_n^{PEO} the PEO block number-average molecular weight, and ρ_{PEO} the PEO amorphous density (1.124 g cm^{-3}).²³ From this calculation, the thickness of the PLLA crystal is between 8 and 10 nm, and each PEO rich layer is between 1 and 2 nm (Table 5). A comparison between the PLLA crystallizable block length and the computed crystal thickness indicates that the PLLA chains are folded inside the lozenge shape crystals and the number of folds increases with the molecular weight of the PLLA block, as expected. The calculated value is an average value. Nevertheless, Xu *et al.*²⁹ claimed that lamella are always thicker in the centre

region than at the growth front. In addition, heterogeneities in crystal thickness do not disappear with time or with the age of the crystal. Zhang *et al.*³⁰ studied polyethylene single crystals consisting of folded chains that are always in a nonequilibrium state, even if they are faceted. For low-molecular weight polyethylene the formation of the well known “Swiss-cheese” like morphology with randomly distributed holes of varying sizes within the annealed single crystal was observed. Hong *et al.*⁵¹ showed the capabilities of solid state NMR and isotope labeling for revealing: chain trajectory in melt and solution-grown crystals; conformation of the folded chains in single crystals, self-folding in the early stage of crystallization and unfolding of the folded chains under stretching.

AFM study with variable temperatures

In order to elucidate more clearly the type of structure formed by the PEO block after PLLA thin films crystallization, AFM tests were performed, using a hot stage, and two steps of isothermal crystallization were applied to each sample: a first step at 100 °C to promote the crystallization of the PLLA block, and a second step at 30 °C to promote the crystallization of the PEO block. After both blocks were isothermally crystallized in sequence, they were heated, using the AFM hot stage, to 70 °C to melt the PEO block crystals. When heating the samples, it is also possible that PLLA folded crystals are annealed. Fig. 7–9 present the changes in morphology and thickness of the samples as a function of temperature for several compositions.

Fig. 7 shows, for block copolymer $\text{EO}_{50}^5\text{LA}_{50}^5$, AFM images of the crystals formed after each crystallization step was applied. Lozenge-shaped crystals were obtained at 100 °C (Fig. 7.a.1, a.2 and a.3) and a new layer (most probably a PEO crystalline layer) appeared nucleated on the edges of the lozenge-shaped PLLA crystals after 15 h of crystallization at 30 °C (Fig. 7.b.1, b.2 and b.3, see arrows).

The traces shown in Fig. 7.c.1 and c.2 indicate that the initial crystal (in green) had a thickness of 18 nm, while the additional treatment at 30 °C lead to a shallow step (shaded in blue) with a thickness of about 12 nm. Fig. 7.d.1 and d.2 are schematic cartoons that represent in green color PLLA block chains and crystals and in blue color PEO block chains and crystals. PEO crystals probably grew at the edge and top of the pre-existing PLLA crystals.

Cheng *et al.*^{52,53} claimed on the basis of time-resolved synchrotron small-angle X-ray scattering (SAXS) and differential scanning calorimetry (DSC) experiments that non integral-folding chain (NIF) crystals form in low molecular weight poly(ethylene oxide) (PEO) fractions. These crystals grow first as a transient state, and integral-folding chain (IF) crystals form later through an isothermal thickening or thinning process. Hong *et al.*⁵¹ showed the capabilities of solid state NMR and isotope labeling for revealing: chain trajectory in melt and solution-grown crystals; conformation of the folded chains in single crystals, self-folding in the early stage of

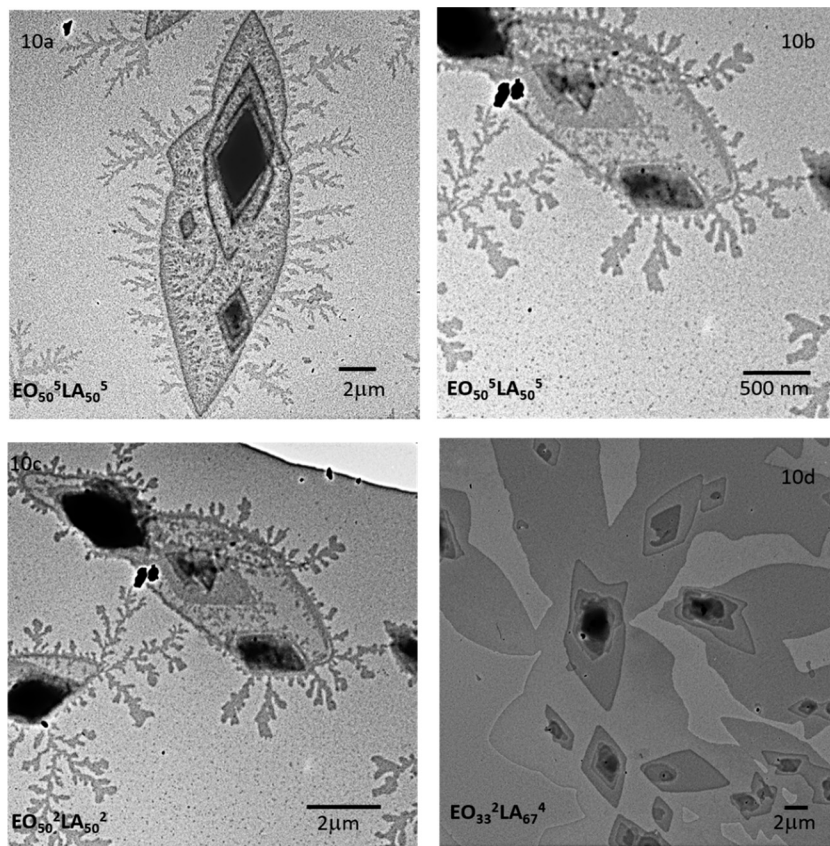


Fig. 10 TEM observations of single crystals and dendritic crystals for PEO-*b*-PLLA block copolymers, that are far from the 120° value expected for lozenge PLLA type crystals with $\{110\}$ growing faces. Smaller lozenge shaped crystals, found on top of the lenticular crystals, are constructed by screw dislocations and exhibit 129° angles, a value closer to the 120° reported for PLLA single crystals. The edges of the single crystals tend to be smooth and no striations were observed on their surface. a) $\text{EO}_{50}^5\text{LA}_{50}^5$, b) $\text{EO}_{50}^5\text{LA}_{50}^5$, c) $\text{EO}_{50}^2\text{LA}_{50}^2$, and d) $\text{EO}_{33}^2\text{LA}_{67}^4$. The magnification is different from one image to the other and is indicated by a scale bar.

crystallization and unfolding of the folded chains under stretching.

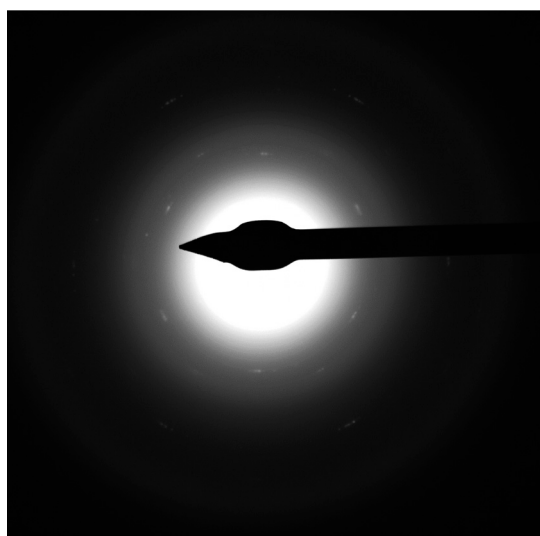


Fig. 11 Electron diffraction pattern for $\text{PEO}_{33}^2\text{LA}_{67}^4$ block copolymer after two types of isothermal crystallization as in Fig. 10.

For block copolymer $\text{EO}_{33}^2\text{LA}_{67}^4$, two series of experiments are shown in Fig. 8. In Fig. 8.a a combination of lozenge-shaped PLLA crystals with second PEO layers were obtained after the two isothermal steps were performed (first at 100°C and then at 30°C).

Fig. 8.b shows the morphology after heating to 70°C to promote the melting of PEO crystals. Fig. 8.c shows evidences of changes in the cross sections of the films with temperature. During the isothermal step at 70°C (melting step for PEO crystals), a reduction in the width or transversal section of the layer at both edges takes place (green trace vs blue shadow trace) as well as in the fold surface of the PLLA lozenge shape crystal.

Fig. 8.d shows the PLLA lozenge shape crystal for PLLA block at 100°C . Fig. 8.e and f correspond to the $\text{EO}_{33}^2\text{LA}_{67}^4$ height and amplitude images at room temperature after the two steps of isothermal crystallization respectively (the presence of a new structure is indicated by an arrow, being clearer in the amplitude image).

Subsequent heating to 70°C illustrates that the structures formed at 30°C disappear or change when the sample is heated to 70°C (see evolution of AFM height traces in Fig. 8. g and h). This behaviour can be interpreted as the melting of

small dendritic crystals of the PEO block when the sample is heated (TEM results in section 3.5 will show more clearly the characteristics of the PEO block crystals). The changes in the profile of the sample are related to rearrangement processes of PLLA block crystals when temperature is increased and to the melting of PEO dendritic crystals. Similar evidence was obtained with $\text{EO}_{29}^2\text{LA}_{71}^5$ (not shown here). Fig. 9 also shows the crystallization of the PLLA block within $\text{EO}_{20}^2\text{LA}_{80}^8$ (a copolymer richer in PLLA than previous samples). In this case, the observed structures are lozenge-shaped crystals after the two isothermal crystallization steps (100 °C + 30 °C). In fact, very similar structures are observed when heating the sample to 70 °C (Fig. 9.a vs. b). Fig. 9.c does not show a significant change in the height trace or lateral dimensions during the isothermal step at 30 °C, or after heating to 70 °C. Therefore, the PEO block must be completely amorphous in this case at all the temperatures evaluated.

TEM study after isothermal crystallization

Fig. 10 shows TEM images obtained after a two step crystallization process for samples $\text{EO}_{50}^5\text{LA}_{50}^5$, $\text{EO}_{50}^2\text{LA}_{50}^2$ and $\text{EO}_{33}^2\text{LA}_{67}^4$. For $\text{EO}_{50}^5\text{LA}_{50}^5$, the sample was isothermally crystallized for 3 h at 100 °C followed by 18 h at 5 °C. A complex structure is observed with two types of crystals (Fig. 10.a): the first ones are multilayered lozenge-shaped PLLA single crystals; the second ones are dendritic crystals nucleated at the edge of the PLLA crystals, as well as small dendritic-like structures on the top surface of the lozenge PLLA single crystals. The dendritic crystals are probably formed by the PEO block chains during the crystallization process at 5 °C, after the PLLA block crystallization took place at 100 °C. However, the lateral length of the dendritic crystals is of the order of a few microns. The degree of crystallinity obtained by DSC for the bulk PLLA block and PEO block are 35 and 73%, respectively.

Therefore, PEO dendritic crystals are probably composed by PEO chains that are covalently linked to PLLA chains belonging to both crystallized PLLA and amorphous PLLA blocks. The contribution of both types of molecules can explain the large lateral length of PEO dendritic crystals.

The shape of the largest PLLA structure is lenticular. This type of growth is reported for the case of single crystals of polyethylene and polyesters in good solvents or when using low supercoolings.^{54–56} It is due to a faster growth rate of the {100} face as compared to that of the {110} faces and, in Fig. 10.a, it is reflected by angles between growing faces of 151°.

Fig. 10.b shows a TEM micrograph for $\text{EO}_{50}^5\text{LA}_{50}^5$, after the sample was isothermally crystallized for 3 h at 100 °C, followed by 18 h at 30 °C. In this case, fewer dendritic crystals are observed for the PEO block, as compared to Fig. 10.a where the isothermal crystallization temperature for the PEO block was much lower (5 °C).

Fig. 10.c shows a similar morphology to that of Fig. 10.a, and corresponds to a lower molecular weight copolymer, *i.e.*,

$\text{EO}_{50}^2\text{LA}_{50}^2$ (the crystallization conditions were 90 °C for 3 h and 5 °C for 18 h). Again, the PLLA block structures observed are lenticular-shaped, lozenge-shaped and lozenge-multistage-shaped crystals, and the PEO block exhibits a dendritic structure. These structures grow on top of the basal surface of the PLLA block crystals and, in adjacent areas, at the edges of the PLLA crystals. For the $\text{EO}_{33}^2\text{LA}_{67}^4$ block copolymer, Fig. 10.d shows lozenge-shaped crystals after isothermal crystallization for 3 h at 100 °C and 18 h at 30 °C. Here, no evidences of dendritic PEO crystals are observed. Nevertheless, Fig. 11 shows the electron diffraction pattern of $\text{EO}_{33}^2\text{LA}_{67}^4$ containing six spots with hexagonal symmetry, corresponding to the PLLA crystal pseudo-orthorhombic α phase ($a = 1.06$ nm, $b = 0.6$ nm, $c = 2.88$ nm (ref. 57)) as well as four weaker spots corresponding to the reflection of the PEO block monoclinic crystals ($a = 0.805$ nm, $b = 1.304$ nm, $c = 1.948$ nm and $\beta = 125.4^\circ$ (ref. 58)). The PEO block signals have the forms of small arcs which can be attributed to the presence of small crystals with different orientations.

Conclusions

The effect of composition and crystallization conditions on the behavior of double crystalline poly (ethylene oxide-*b*-lactide) (PEO-*b*-PLLA) diblock copolymers was evaluated. The PEO block was kept constant at 2 kg mol⁻¹, the molecular weight of the poly(l-lactide) PLLA block ranges from 2 to 20 kg mol⁻¹ and its content in the synthesized copolymers varies from 50 to 91%.

The DSC study of the crystallization process of the double crystalline diblock copolymers PEO-*b*-PLLA in the bulk allowed the observation of a complex interaction: 1. PEO blocks exert a synergistic combination of heterogeneities donation and plasticizing action on the PLLA block crystallization.² PLLA blocks exert two opposing effects over PEO block crystallization: a nucleation action over PEO block crystallization and also topological and geometrical constraints for PEO block crystallization. When PEO contents are between 29 and 50% the contribution of nucleation action is the most important for PEO block crystallization. For copolymers with PEO content equal or below 20%, the topological and geometrical constraints are the most important contribution.

Morphological study in thin films by AFM and TEM of isothermal crystallization from the melt shows PLLA lozenge shaped crystals. Nevertheless, the amount of PEO in the system affects the shape of the single crystals. The better defined PLLA lozenge shaped crystals are observed in block copolymers with PEO contents between 29 and 50%. The PEO block acts as a diluent for the PLLA crystallization process. Block copolymers with PEO contents equal or smaller than 20% form distorted PLLA single crystals when crystallized from the melt. However, upon increasing the PEO content in the system to 33% (by blending or copolymerization), the distortions disappear and the angle between the {110} growth faces changes from 140° to 121°; PEO incorporation can therefore tailor the rate and morphology of PLLA block

crystallization. In addition, TEM and AFM studies of the isothermal crystallization of a series of PEO-*b*-PLLA block copolymers allowed the observation of PLLA single crystals and PEO dendritic crystals on the folding surface and edges of the PLLA single crystals. The morphology therefore consists of a central structure of lozenge-shaped PLLA crystals sandwiched by a semi-crystalline layer of PEO dendritic crystals and mixed or partially miscible amorphous regions.

Acknowledgements

M. L. Arnal acknowledges the support from Université de Montréal and Universidad Simón Bolívar for her sabbatical year. The authors would like to thank the National Sciences and Engineering Research Council (NSERC) of Canada, le Fonds Québécois de la Recherche sur la Nature et les Technologies (FQRNT) and NanoQuébec for supporting this study. J. M. Raquez is a research fellow from the Belgian FRS-FNRS research agency. A. J. Müller would like to acknowledge funding through grant Mineco MAT2014-53437-C2-P.

References

- I. W. Hamley, in *Developments in Block Copolymer Science and Technology*, ed. I. W. Hamley, Wiley, West Sussex, 2004, ch. 1, pp. 1–30.
- I. W. Hamley, *The Physics of Block Copolymers*, Oxford University Press, Oxford, 1998.
- N. Hadjichristidis, S. Pispas and G. A. Floudas, *Block Copolymers: Synthetic Strategies, Physical Properties, and Applications*, Wiley, New Jersey, 2003.
- A. J. Müller, M. L. Arnal and V. Balsamo, in *Lecture Notes in Physics: Progress in Understanding of Polymer Crystallization*, ed. G. Reiter and G. R. Strobl, Springer-Verlag, Berlin, 2007, ch. 13, vol. 714, p. 229.
- Y. L. Loo and R. Register, in *Developments in Block Copolymer Science and Technology*, ed. I. W. Hamley, Wiley, West Sussex, 2004, ch 6, pp. 213–242.
- R. V. Castillo and A. J. Müller, *Prog. Polym. Sci.*, 2009, **34**, 516.
- W. N. He and J. T. Xu, *Prog. Polym. Sci.*, 2012, **37**, 1350.
- S. Slomkowski, *Macromol. Symp.*, 2007, **253**, 47.
- Y. Wang, *US Pat. App.*, 13/279809, 2011.
- I. Rashkov, N. Manolova, S. M. Li, J. L. Espartero and M. Vert, *Macromolecules*, 1996, **29**, 50.
- C. G. Mothé, W. S. Drumond and S. H. Wang, *Thermochim. Acta*, 2006, **445**, 61.
- J. Sun, Z. Hong, L. Yang, Z. Tang, X. Chen and X. Jing, *Polymer*, 2004, **45**, 5969.
- S. Huang, S. Jiang, L. An and X. Chen, *J. Polym. Sci., Part B: Polym. Phys.*, 2008, **46**, 1400.
- S. Huang, H. Li, S. Jiang, X. Chen and L. An, *Polym. Bull.*, 2011, **67**, 885.
- C. I. Huang, S.-H. Tsai and C.-M. Chen, *J. Polym. Sci., Part B: Polym. Phys.*, 2006, **44**, 2438.
- K. Kim, S. Chung, I. Chi, M. Kim and J. Yoon, *J. Appl. Polym. Sci.*, 1999, **72**, 341–348.
- J. Yang, T. Zhao, J. Cui, L. Liu, Y. Zhou and G. Li, *J. Polym. Sci., Part B: Polym. Phys.*, 2006, **44**, 3215.
- D. Shin, K. Shin, K. A. Aamer, G. N. Tew, T. P. Russell, J. H. Lee and J. Y. Jho, *Macromolecules*, 2005, **38**, 104.
- C. Cai, L. Wang and C.-M. Dong, *J. Polym. Sci., Part A: Polym. Chem.*, 2006, **44**, 2034.
- J. Yang, T. Zhao, Y. Zhou, L. Liu, G. Li, E. Zhou and X. Chen, *Macromolecules*, 2007, **40**, 2791.
- J. Yang, Y. Liang, J. Luo, C. Zhao and C. C. Han, *Macromolecules*, 2012, **45**, 4254.
- J. Yang, Y. Liang, W. Shi, H. Lee and C. C. Han, *Polymer*, 2013, **54**, 3974.
- F. Meyer, J.-M. Raquez, P. Verge, I. Martínez de Arenaza, B. Coto, P. Van Der Voort, E. Meaurio, B. Dervaux, J.-R. Sarasua, F. Du Prez and Ph. Dubois, *Biomacromolecules*, 2011, **12**, 4086.
- J. Brandrup, *Polymer Handbook*, ed. E. H. Immergut, 3rd edn, Wiley, New York, 1989, pp. IV-72.
- J. F. Turner, A. Riga, A. O'Connor, J. Zhang and J. Collis, *J. Therm. Anal. Calorim.*, 2004, **75**, 257.
- B. Fillon, J. C. Wittman, B. Lotz and A. Thierry, *J. Polym. Sci., Part B: Polym. Phys.*, 1993, **31**, 1383.
- A. T. Lorenzo, M. L. Arnal, J. J. Sánchez and A. J. Müller, *J. Polym. Sci., Part B: Polym. Phys.*, 2006, **44**, 1738.
- R. M. Michell, A. Mugica, M. Zubitur and A. J. Müller, Self-Nucleation of Crystalline Phases within Homopolymers, Polymer Blends, Copolymers, and Nanocomposites, *Adv. Polym. Sci.*, 2016, DOI: 10.1007/12_2015_327.
- J. Xu, Y. Ma, W. Hu, M. Rehahn and G. Reiter, *Nat. Mater.*, 2009, **8**, 348.
- B. Zhang, J. Chen, M. C. Baier, S. Mecking, R. Reiter, R. Mülhaupt and G. Reiter, *Macromol. Rapid Commun.*, 2015, **36**, 181.
- G. Reiter and S. Jens-Uwe, *Phys. Rev. Lett.*, 1998, **80**, 3771.
- G. Reiter and S. Jens-Uwe, *J. Chem. Phys.*, 2000, **112**, 4376.
- S. Hölzer, T. N. Büttner, R. Schulze, M. M. Arras, F. H. Schacher, K. D. Jandt and U. S. Schubert, *Eur. Polym. J.*, 2015, **68**, 10.
- K. Adamska and A. Voelkel, *J. Chromatogr. A*, 2006, **1132**, 260.
- D. Karst and Y. Yang, *J. Appl. Polym. Sci.*, 2005, **96**, 416.
- M. W. Matsen and F. S. Bates, *Macromolecules*, 1996, **29**, 1091.
- R. V. Castillo, A. J. Müller, J.-M. Raquez and P. Dubois, *Macromolecules*, 2010, **43**, 4149.
- N. D. Zhou, J. Sun, J. Shao, X. Bian, S. Huang, G. Li and X. Chen, *Polymer*, 2015, **80**, 123.
- U. W. Gedde, *Polymer Physics*, Springer Science & Business Media, Berlin, 1995, pp. 143–210.
- H. Frensch, P. Harnischfeger and B.-J. Jungnickel, in *Multiphase Polymers: Blends and Ionomers*, ed. L. A. Utracki and R. A. Weiss, ACS Symposium Series, Washington DC, 1989, ch. 5, p. 101.

- 41 M. L. Arnal, M. E. Matos, R. A. Morales, O. O. Santana and A. J. Müller, *Macromol. Chem. Phys.*, 1998, **199**, 2275.
- 42 Y. He, B. Zhu, W. Kai and Y. Inoue, *Macromolecules*, 2004, **37**, 3337.
- 43 A. J. Müller, V. Balsamo, M. L. Arnal, T. Jakob, H. Schmalz and V. Abetz, *Macromolecules*, 2002, **35**, 3048.
- 44 R. M. Michell, A. J. Müller, V. Castelletto, I. Hamley, G. Deshayes and Ph. Dubois, *Macromolecules*, 2009, **42**, 6671.
- 45 B. Fillon, B. Lotz, A. Thierry and J. C. Wittmann, *J. Polym. Sci., Part B: Polym. Phys.*, 1993, **31**, 1395.
- 46 V. Balsamo, A. J. Müller and R. Stadler, *Macromolecules*, 1998, **31**, 7756.
- 47 M. L. Arnal, F. López-Carrasquero, E. Laredo and A. J. Müller, *Eur. Polym. J.*, 2004, **40**, 1461.
- 48 T. Iwata and Y. Doi, *Macromolecules*, 1998, **31**, 2461.
- 49 W. Hoogsten, A. R. Postemo, A. J. Pennings, G. ten Brinke and P. Zugenmaier, *Macromolecules*, 1990, **23**, 634.
- 50 W. Y. Chen, C. Y. Li, J. X. Zheng, P. Huag, L. Zhu, Q. Ge, R. P. Quirk, B. Lotz, L. Deng, C. Wu, E. L. Thomas and S. Z. D. Cheng, *Macromolecules*, 2004, **37**, 5292.
- 51 Y.-L. Hong, W. Chen, S. Yuan, J. Kang and T. Miyoshi, *ACS Macro Lett.*, 2016, **5**, 355.
- 52 S. Z. D. Cheng and J. Chen, *J. Polym. Sci., Part B: Polym. Phys.*, 1991, **29**(3), 311.
- 53 S. Z. D. Cheng, J. Chen, A. Zhang and D. P. Heberer, *J. Polym. Sci., Part B: Polym. Phys.*, 1991, **29**(3), 299.
- 54 M. T. Casas, J. Puiggali, J.-M. Raquez, Ph. Dubois, M. E. Córdova and A. J. Müller, *Polymer*, 2011, **52**, 5166.
- 55 S. Gestí, M. T. Casas and J. Puiggali, *Polymer*, 2007, **48**, 5088.
- 56 S. Gestí, A. Almontassir, M. T. Casas and J. Puiggali, *Polymer*, 2004, **45**, 8845.
- 57 W. Hoogsten, Postemo A. R., nnJ. Pennings, G. ten Brinke and P. Zugenmaier, *Macromolecules*, 1990, **23**, 634–642.
- 58 Y. Takahashi and H. Tadokoro, *Macromolecules*, 1973, **6**, 672–675.